ACI MATERIALS JOURNAL TECHNICAL PAPER

Title No. 121-M49

Preparation of Performance-Enhanced Alkali-Activated Slag by Using L-Ascorbic Acid

by Peiyuan Chen, Chunning Pei, Liheng Zhang, Shangkun Li, and Jialai Wang

The applications of alkali-activated slag (AAS) face challenges such as poor workability, rapid setting, and high autogenous shrinkage, which require chemical admixtures (CAs) to adjust the performance of AAS. Unfortunately, there are limited specific CAs available to tune AAS properties. To address this gap, this study proposes using a ubiquitous, naturally occurring compound, L-ascorbic acid (LAA), as a multifunctional performance-enhancing additive for AAS to overcome the major challenges of AAS. The findings showed that LAA can function as a retarder, plasticizer, strength enhancer, and autogenous shrinkage reducer for AAS. When 0.5% LAA was added, the compressive strengths of AAS mortars at 3 and 28 days increased by 28.9% and 19.6%, respectively, and the 28-day autogenous shrinkage decreased by 43.1%. Both surface adsorption and ion complexation have been confirmed as the working mechanisms of LAA in hydrated AAS.

Keywords: alkali-activated slag (AAS); autogenous shrinkage; complex; L-ascorbic acid (LAA); setting time.

INTRODUCTION

The production of ordinary portland cement (OPC) has been regarded as an extremely energy-intensive process, and approximately 7% of anthropogenic greenhouse gas emissions are generated.[1] This presents an unsustainable burden in terms of energy consumption and CO_2 emissions, particularly considering that over 4.4 billion tonnes (4.9 billion tons) of OPC are produced annually worldwide. To this end, researchers are exploring greener binders with lower carbon emissions to reduce the carbon footprint of the prepared concrete materials. One such promising option is alkali-activated slag (AAS), which uses slag as the primary precursor without requiring clinker and calcination processes. It has been reported that AAS has the potential to reduce CO_2 emissions by 80% when compared to OPC on a binder-to-binder basis or over 60% when compared to concrete on a concrete-to-concrete basis.[2-4] Through appropriate proportioning, AAS can exhibit material properties comparable to those of OPC.[5]

However, the practical application of AAS still faces challenges due to poor workability, rapid setting, and high autogenous shrinkage of this material.[6,7] In particular, the high shrinkage of AAS increases its risk of cracking, which decreases the durability characteristics of the AAS system.[7] To overcome these issues, chemical admixtures (CAs) are necessary to adjust the performance of AAS. However, there are limited CAs specifically developed for AAS, and most studies have relied on CAs originally developed for OPC-based materials to modify the properties of AAS. One example of such CAs is high-range water-reducing admixture (HRWRA), which can be adsorbed on cement grains due to its abundant hydrophilic groups and negatively charged properties.[8] The adsorbed HRWRA can block reactive sites of cement, leading to electrostatic and/or steric repulsion effects and improving cement dispersion and fluidity.[9,10] Moreover, the addition of HRWRA into concrete can also improve the adhesion, cohesion, strength, and durability of cement paste and concrete.[8,10] However, the use of HRWRA in AAS is complicated by compatibility issues due to the negative charge of slag particles.[11] This can limit the efficiency of HRWRA adsorption on slag particles, which is primarily determined by the number of charged sites in the backbone of the HRWRA.[12] In an AAS system, HRWRA molecules are also influenced by the high pH value and ionic strength of the pore solution.[13,14] Modifying the molecular weight, side-chain length, and density of HRWRAs represents a potential solution to enhance their compatibility with AAS.[12] Moreover, the highly alkaline conditions of AAS can accelerate the decomposition of HRWRAs, posing a threat to their stability.[11] As a result, a larger amount of HRWRA may be required to achieve the desired performance of AAS compared to the OPC system, and the compressive strength and durability could be negatively affected.[5] Therefore, the development of novel and more effective admixtures is crucial for the advancement and widespread application of AAS.

Recently, a study by the authors showed that L-ascorbic acid (LAA) can function as a set retarder for calcium sulfoaluminate cement (CSA).[15] It is a naturally occurring compound found in various fruits and vegetables and exhibits a retarding effect by adsorbing onto CSA grains and forming a complex with Ca^{2+}. The use of LAA not only obviously extended the setting time of CSA but also enabled the formation of refined pore structures of CSA mortars. It can be seen that two admixtures, HRWRA and LAA, exhibited excellent properties when applied to concrete systems, such as improved workability, increased strength, dense microstructure, and enhanced durability. Moreover, another potential advantage of incorporating LAA in cementitious materials is its ability to inhibit corrosion in steel. Fuchs-Godec et al.[16] demonstrated that LAA, at concentrations of 10^{-2} and 10^{-3} M, displayed favorable inhibition efficiency

ACI Materials Journal, V. 121, No. 5, September 2024.

MS No. M-2023-330.R1, doi: 10.14359/51742041, received June 21, 2024, and reviewed under Institute publication policies. Copyright © 2024, American Concrete Institute. All rights reserved, including the making of copies unless permission is obtained from the copyright proprietors. Pertinent discussion including author's closure, if any, will be published ten months from this journal's date if the discussion is received within four months of the paper's print publication.

Table 1—Chemical composition of GGBFS analyzed by XRF

Al_2O_3, %	SiO_2, %	CaO, %	Fe_2O_3, %	MgO, %	SO_3, %	K_2O, %	Other, %
16.08	27.18	45.15	0.37	7.78	2.24	0.35	0.85

Table 2—Mixture proportions and cost of AAS mortars

Mixtures	GGBFS	Sand	Water	NaOH	LAA	Cost
	Unit weight, kg/m^3					Unit ton, USD/tonne
LAA0	793.2	972.5	309.2	86.3	0	59.8
LAA2	793.2	972.5	309.2	86.3	1.6	62.0
LAA5	793.2	972.5	309.2	86.3	4.0	65.3
LAA7	793.2	972.5	309.2	86.3	5.6	67.4
LAA10	793.2	972.5	309.2	86.3	7.9	70.5

Note: 1 kg/m^3 = 0.06242 lb/ft^3; 1 tonne = 2204.62 lb.

for stainless steel (SS) type X4Cr13 in an HCl solution, with higher LAA concentrations leading to increased inhibition efficiency.[17] This effect is attributed to the chemical reactivity of the hydroxyl groups on the enol-form ring of LAA, which provide sites for the complexation or crosslinking of macromolecules or metal ions.[18,19]

Based on the findings of these studies, this research proposes that LAA can serve as a multifunctional performance-enhancing additive (PEA) for AAS. Compared to existing CAs derived from fossil fuels, LAA offers clear environmental advantages as it is renewable and readily available in various plants and microorganisms. Additionally, LAA is nontoxic and does not pose a threat to human health or the ecosystem. When added to AAS at a low dosage, LAA can fulfill multiple roles traditionally performed by separate CAs, including acting as a retarder, plasticizer, autogenous shrinkage reducer, and corrosion inhibitor. This multifunctional additive has the potential to address the three major challenges that currently limit the field application of AAS. To this end, the influences of LAA on the setting time, fluidity, hydration kinetics, hydration products, compressive strength, autogenous shrinkage, and pore structure of AAS were investigated to reveal the underlying working mechanisms.

RESEARCH SIGNIFICANCE

The study's significance lies in proposing the use of a naturally occurring, widely available compound as a multifunctional additive to improve the performance of AAS. It can also inspire the development of novel additives for AAS using the molecule of LAA, considering its chelating ability with ions.

EXPERIMENTAL PROCEDURE

Materials

Ground-granulated blast-furnace slag (GGBFS) with an apparent density and specific surface area of 2800 kg/m^3 (174.78 lb/ft^3) and 650 m^2/kg, respectively, was sourced from a company in China. Table 1 shows its chemical composition analyzed by an X-ray fluorescence (XRF) spectrometer. The GGBFS exhibited a highly vitreous nature and high reactivity with small amounts of melilite, as indicated by the X-ray diffraction (XRD) pattern shown in Fig. 1. Analytically pure NaOH and LAA were sourced from a company in China. River sand with a fineness modulus of 2.6 and tap water were used.

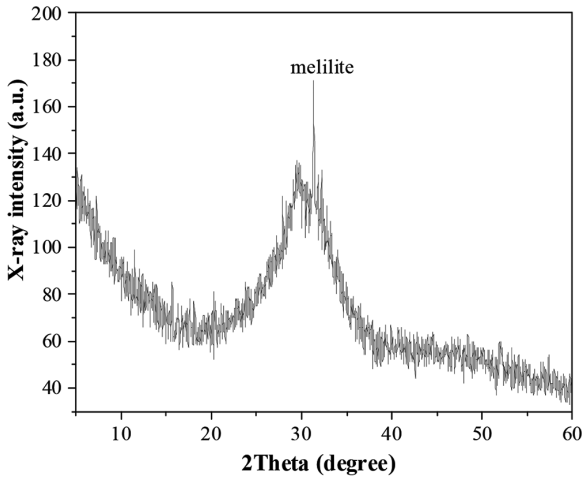

Fig. 1—XRD pattern of GGBFS.

Proportions and mixing procedure

Table 2 presents the mixture proportions and cost of AAS mortars. It can be seen that the addition of LAA slightly increases the cost of producing AAS mortar, which is understandable because additional admixtures are added. Five different dosages of LAA were used as admixtures for AAS, namely 0.0, 0.2, 0.5, 0.7, and 1% by mass of GGBFS. These mortars were named based on their LAA dosage (LAA0, LAA2, LAA5, LAA7, and LAA10), with a consistent water-cement ratio (*w*/*c*) of 0.40. In a typical production of LAA-added AAS mortar, room-temperature NaOH solution (molarity concentration of 6.3 mol/L) was first prepared using 75% of the mixing water, and LAA was dissolved in the other 25% of mixing water. Then, GGBFS and sand were mixed by a mixer for 5 minutes, and the two solutions were mixed quickly and added into the mixer, followed by low-speed mixing for 1 minute and then high-speed mixing for an additional 2 minutes. Additionally, paste samples were also prepared using the same method but without the inclusion of sand.

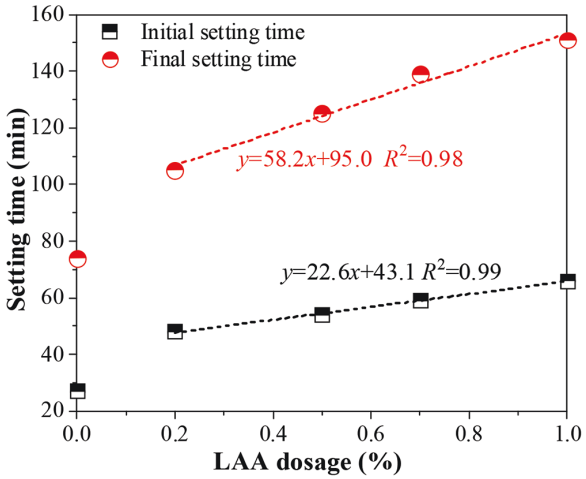

Fig. 2—Setting times of AAS pastes.

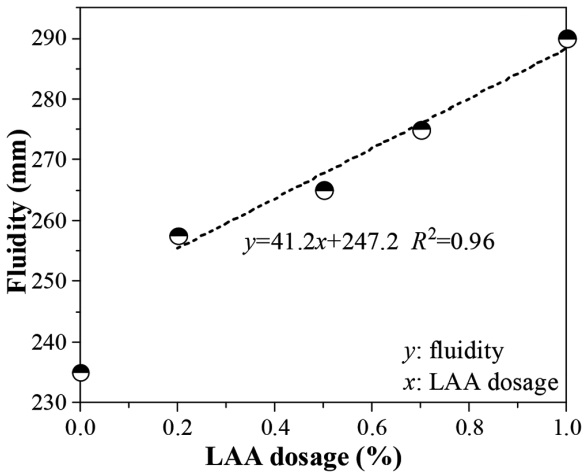

Fig. 3—Fluidity of AAS mortars. (Note: 1 mm = 0.039 in.)

Test methods

A Vicat apparatus was applied to measure the setting times of AAS pastes in a curing room maintained (23 ± 2°C [73.4°F] and >95% relative humidity [RH]) according to ASTM C191-99.[20]

The workability of the AAS mortar samples was assessed by measuring their fluidity using a fluidity tester, following ASTM C1437-20.[21]

The compressive strength measurements of AAS mortars were carried out at 3, 7, and 28 days after hydration, using a 300 kN (6.75×10^4 lbf) load cell with a loading rate of 0.5 kN/s (112.44 lbf/s). Cubic samples with a size of 50 x 50 x 50 mm (2 x 2 x 2 in.) were cast and cured in the curing room. The results were reported based on triplicate samples.

The autogenous shrinkage of AAS was measured using corrugated tubes (420 mm [16.53 in.] in length and 29 mm [1.14 in.] in diameter) according to ASTM C1698-09(2014).[22] The data were recorded using a dilatometer bench equipped with a digital gauge at one end, starting from the final setting time of the mortar and continuing until 28 days. The results were reported based on triplicate samples, which were cured in the curing room.

The pore structures of 28-day AAS mortars were studied using mercury intrusion porosimetry (MIP). Prior to analysis, the samples were soaked in isopropanol for at least 7 days to prevent further hydration of GGBFS and then vacuum-dried.

The hydration kinetics of AAS were studied using an isothermal calorimeter. Approximately 6 g (0.0132 lb) of paste was prepared for each mixture, and the samples were mixed within glass bottles in the calorimeter chamber to capture all possible hydration heat flow. The temperature of the chamber was maintained at 23 ± 2°C (73.4°F) during the experiment, and heat flow was recorded for pastes every 1 minute until 72 hours.

A high-resolution XRD (Cu-Kα, 40 kV, 20 mA) was applied to analyze the hydration products of AAS with a scan range of 5 to 60 degrees. The AAS paste samples used for the analysis of hydration products were first soaked in isopropanol for at least 7 days to cease the hydration of the slag. They were then pulverized into particles less than 75 µm (2.9×10^{-3} in.) using an agate grinder before analysis.

An inductively coupled plasma optical emission spectrometer (ICP-OES) was applied to analyze the pore solution of AAS. In a typical procedure for preparing the aqueous phase, 10 g (0.022 lb) of deionized (DI) water was initially mixed with 0.11 g (2.42×10^{-4} lb) of NaOH, and LAA (0, 0.002, 0.005, 0.007, and 0.01 g [0, 4.40×10^{-6}, 1.10×10^{-5}, 1.54×10^{-5}, 2.20×10^{-5} lb]) was then added to prepare LAA-NaOH solutions. Subsequently, 1 g (2.2×10^{-3} lb) of GGBFS was added to the LAA-NaOH solutions and mixed to prepare AAS pastes. The mixture was centrifuged for 1 minute at 4000 rpm when hydrated for 5 minutes, 15 minutes, 30 minutes, 1 hour, 2 hours, 4 hours, 6 hours, 12 hours, or 24 hours, and subsequently, it was filtered through a 20 nm (7.8×10^{-7} in.) membrane to obtain the aqueous phase of the hydrating AAS, which was diluted by 1% nitric acid to the measurable range of the instrument. In addition, the total organic carbon (TOC) of the prepared solutions was also analyzed (using a TOC analyzer). Reference solutions were prepared by mixing LAA and DI water to determine the adsorption rate of LAA by solids.

EXPERIMENTAL RESULTS

Setting time

Figure 2 shows the setting times of AAS pastes. The setting time of LAA0 represents the typical rapid-setting characteristics of NaOH-activated AAS, as it sets in 28 minutes. By adding LAA, the quick setting of AAS can be significantly mitigated, as LAA-added AAS pastes have longer setting times than LAA0. The linear regression analysis indicates that the setting times of AAS pastes exhibit an almost linear increase with the dosage of LAA. Compared with LAA0, the setting times of AAS pastes with 0.2 to 1% LAA were prolonged by 77.8 to 144.4% for the initial setting and 41.9 to 104.1% for the final setting, respectively. Therefore, LAA can act as a retarder for AAS.

Fluidity of AAS mortars

Figure 3 presents the fluidity of AAS mortars. It is evident that the addition of LAA results in a nearly linear increase in the fluidity of the mortars. A 9.6 to 23.4% improvement in fluidity can be achieved by using 0.2 to 1% LAA for the

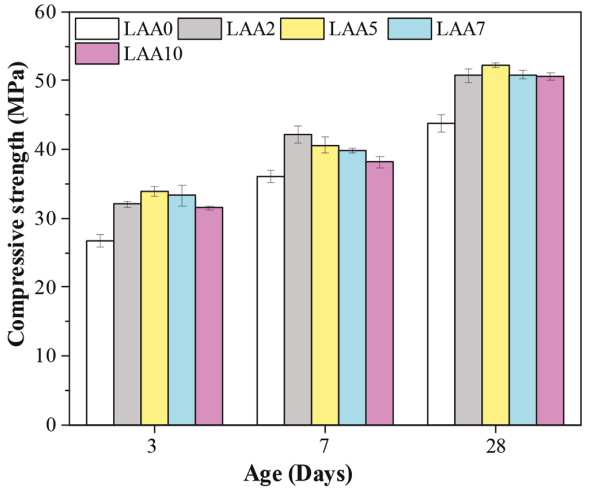

Fig. 4—Compressive strengths of AAS mortars. (Note: 1 MPa = 0.145 ksi.)

AAS mortars, indicating that LAA can be used as a plasticizer for AAS mortars.

Compressive strength of AAS mortars

Figure 4 displays the compressive strengths of AAS mortars, along with the strength increments of LAA-added mortars relative to LAA0. The results indicate that LAA acts as a strength enhancer for AAS mortars, with the compressive strengths of LAA-added mortars surpassing that of LAA0 at all ages. At 3 days, the addition of LAA improves the compressive strengths by 20.0%, 28.9%, 24.7%, and 18.0% for LAA2, LAA5, LAA7, and LAA10, respectively. However, a lower strength improvement is observed for LAA10 by the addition of 1.0% LAA, possibly resulting from the retarding effect of LAA. This retarding effect becomes more pronounced at 7 days, resulting in a slight reduction in the strength improvement with increasing LAA dosage. Nonetheless, all mortars exhibit compressive strengths higher than LAA0 at 28 days, with LAA5 achieving the highest strength improvement of 19.6% over that of LAA0.

Autogenous shrinkage

Figure 5 presents the autogenous shrinkage of AAS mortars. It can be found that the autogenous shrinkage of LAA0 develops rapidly and continues for approximately 28 days to 3083 με without showing any sign of stopping. However, the addition of LAA significantly reduces this shrinkage. As shown in the figure, the autogenous shrinkages of LAA2, LAA5, LAA7, and LAA10 at 28 days are reduced to 2058, 1735, 1503, and 1118 με, respectively. Using a higher dosage of LAA results in a greater reduction in autogenous shrinkage, with LAA10 achieving the highest reduction, where the shrinkage at 28 days is as low as one-third of LAA0. Therefore, LAA can be used effectively as a reducer of autogenous shrinkage for AAS.

Pore structure

The pore structures of the AAS mortars at 28 days were obtained through MIP analysis, and the results are presented

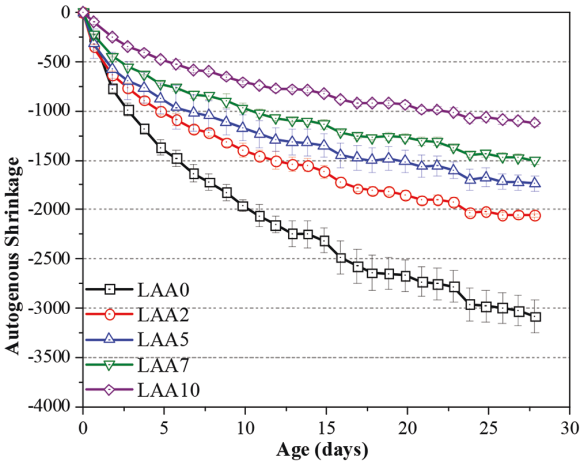

Fig. 5—Autogenous shrinkages of AAS mortars.

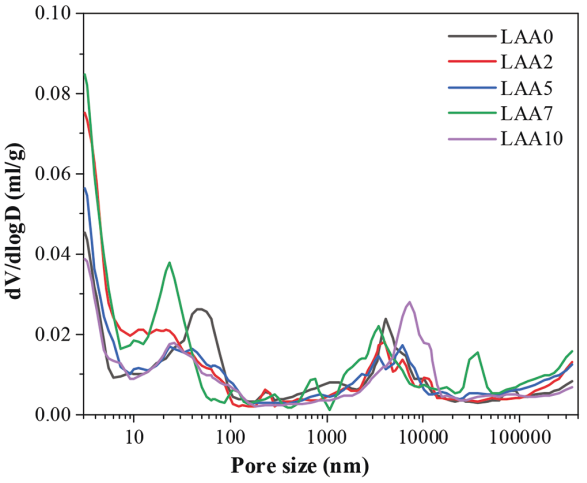

Fig. 6—Pore-size distributions of 28-day AAS mortars. (Note: 1 mL/g = 15.45 oz./lb; 1 nm = 3.94 × 10^{-8} in.)

in Fig. 6. It is evident that the addition of LAA significantly influenced the formation of pores smaller than 100 nm (3.9 × 10^{-6} in.) in AAS mortars. Compared to LAA0, the LAA-added mortars had lower volumes of pores ranging from 20 to 100 nm (7.8 × 10^{-7} to 3.9 × 10^{-6} in.). Because these are large mesopores that affect shrinkage above 80% RH, the reduced volume of these pores indicates the formation of smaller autogenous shrinkage.[23,24] More importantly, reducing these pores densifies the microstructure of the AAS mortars, leading to much higher compressive strength, as revealed by Fig. 4. Figure 6 also reveals that LAA-added mortars have more pores smaller than 30 nm (1.2 × 10^{-6} in.), especially those smaller than 10 nm (3.9 × 10^{-7} in.) when compared to LAA0. Generally, the pores smaller than 10 nm (3.9 × 10^{-7} in.) in AAS materials represent the inherent pores of gel products.[25] The increase in these pores suggests the formation of more hydration products with the presence of LAA.

Hydration kinetics of AAS

The hydration kinetics of AAS with the presence of LAA were analyzed, as shown in Fig. 7. Two exothermic peaks were detected on the curves. The first peak, occurring between 0 and 0.5 hours, can be attributed to the wetting of

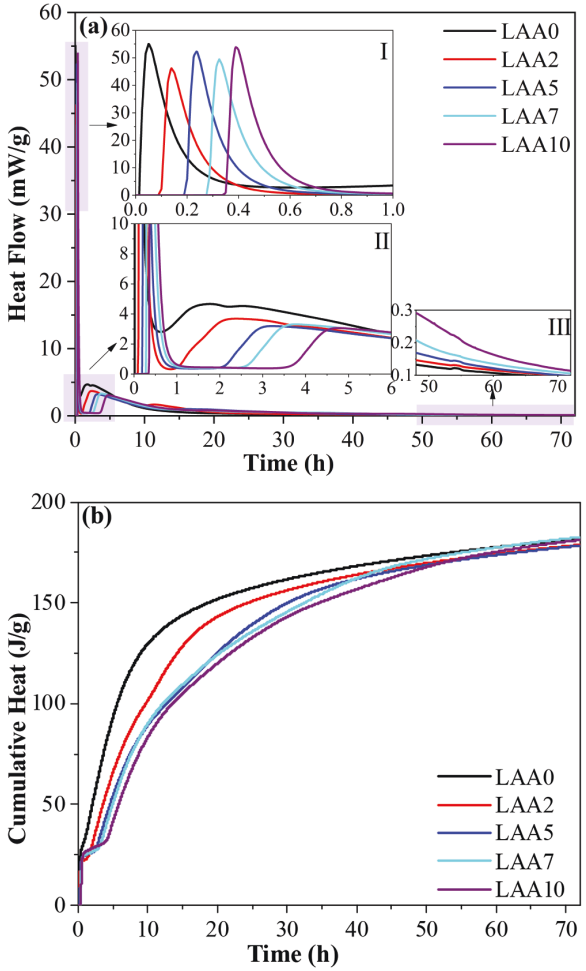

Fig. 7—Isothermal calorimetry results of AAS pastes: (a) heat flow; and (b) cumulative heat. (Note: 1 mW/g = 453.72 mW/lb.)

GGBFS grains, the dissolution of GGBFS upon contact with alkali activators, and the formation of initial complexes.[26] After the initial peak, the hydration of the AAS paste enters an induction period lasting from 1 to 4 hours. During this stage, the precipitation of hydration products, such as calcium-aluminate-silicate-hydrate (C-A-S-H) gels, over the anhydrous slag grains inhibits the hydration process.[27]

The addition of LAA had a notable impact on the hydration heat profiles of AAS pastes. As illustrated in the first close-up in Fig. 7(a), the initial hydration peaks of AAS pastes were delayed by the incorporation of LAA, and this delay increased with the amount of LAA added, revealing that LAA suppressed the dissolution of GGBFS and the formation of initial hydration products. This is consistent with the results of setting time shown in Fig. 2. The retarding effect of LAA on the AAS paste's hydration is further evidenced by the prolonged induction period and reduced thermal flow observed during this period in pastes containing LAA.

The addition of LAA prolonged the induction periods with LAA dosage. For instance, when using 1% LAA, the induction period extends to approximately 2.4 hours. As a result of the prolonged induction period caused by the addition of LAA, the second exothermic peaks of AAS pastes, which signify the end of the acceleration period of hydration, are

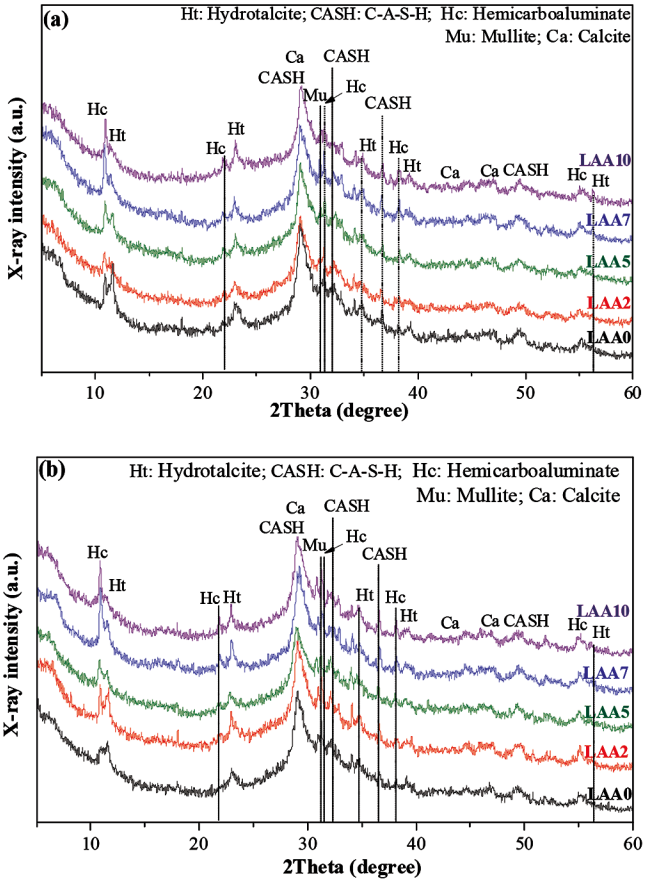

Fig. 8—XRD patterns of AAS pastes: (a) 3 days; and (b) 28 days.

delayed, as depicted in the second close-up in Fig. 7(a). Moreover, the magnitude of this peak is reduced due to the retarding effect of LAA. After the second peak, the AAS paste sample enters the deceleration period, as shown in the third close-up in Fig. 7(a). AAS mixtures containing LAA generate more hydration heat than LAA0 during this period, indicating that the addition of LAA promotes hydration at this stage. The retarding effect of LAA diminishes toward the end of the calorimetry testing, as evidenced by the cumulative hydration heat displayed in Fig. 7(b). This figure illustrates that the cumulative hydration heats of all AAS pastes containing LAA are very close to that of LAA0 by the end of the measurement.

XRD analysis

Figure 8(a) presents the XRD patterns of 3-day AAS pastes. The main hydration product, Al-integrated C-A-S-H, is identified at peaks of $2\theta = 29.0$, 32.2, 36.6, and 49.4 degrees in all pastes. Calcite is also present in the samples, with an intensity peak overlapping with C-A-S-H at $2\theta = 29.0$ degrees. Because no carbonate was detected in the raw GGBFS, the generation of calcite in AAS pastes could be the result of the carbonation of hydroxides during curing.[28] Additionally, an alumina, ferric oxide, monosubstituted (AFm) phase—hemicarboaluminate containing OH^- and CO_3^{2-} as the incorporated interlayer anions—was found.[29] As the dosage of LAA increases, there is a noticeable enhancement in the intensity peak of hemicarboaluminate at $2\theta = 10.8$ degrees.

Because hemicarboaluminate is susceptible to being transformed into monocarboaluminate with longer aging,[30] it is suggested that the addition of LAA may stabilize hemicarboaluminate and slow down its transformation into monocarboaluminate. Moreover, the addition of LAA appears to slightly suppress the formation of hydrotalcite, as indicated by the decreased intensity of peaks at $2\theta = 11.6$ degrees.

Figure 8(b) shows the XRD patterns of 28-day AAS pastes. The same minerals can be found at this age as those identified at 3 days. Similar to 3 days, the peaks at $2\theta = 10.9$, 23.1, and 34.8 degrees, representing hemicarboaluminate, increase with the addition of LAA, while the peak of hydrotalcite becomes weaker with the presence of more LAA.

TG-DTG analysis

Figure 9 shows the thermogravimetric (TG)-derivative thermogravimetry (DTG) results of 28-day AAS pastes. The first peak of the DTG curves, observed at approximately 60°C (140°F), corresponds to the dehydration of loosely bound water in C-A-S-H gels.[31] The endothermic peaks within the temperature ranges of 220 to 425°C (428 to 797°F) and 600 to 800°C (1112 to 1472°F) primarily represent the decomposition of hydrotalcite and calcite, respectively.[32] Comparing LAA0 to samples with added LAA, it can be observed that the samples with LAA exhibited increased mass losses during the heating process up to 800°C (1472°F), and this mass loss increased with higher dosages of LAA, suggesting that the addition of LAA generally promoted the hydration of AAS.

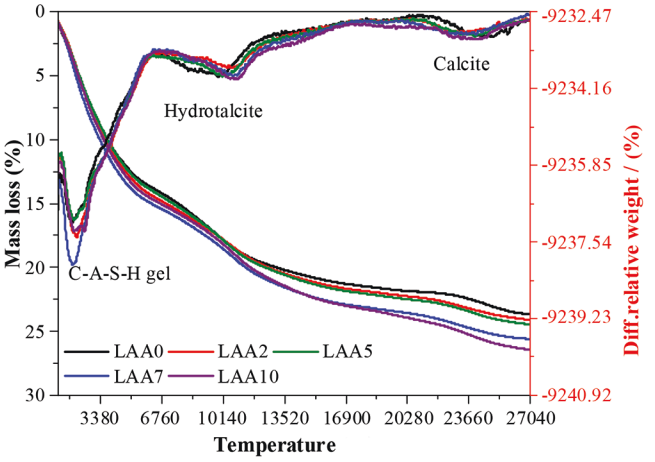

Fig. 9—TG-DTG curves of 28-day AAS pastes. (Note: °F = [°C × 1.8] + 32.)

MECHANISM DISCUSSIONS

Effect of LAA on TOC of aqueous phase of hydrating AAS pastes

Figure 10 illustrates the TOC content of the aqueous phase in AAS pastes over a 24-hour period. The sample with a higher LAA content had a higher TOC, while the sample with no LAA had negligible TOC. For all LAA-containing samples, the TOC exhibited a similar pattern over time. The TOC in all samples dropped by more than half immediately after mixing with the GGBFS and activator, indicating that most of the LAA was adsorbed during the mixing process. Because there are only a few hydration products present in the fresh paste samples at this stage, most of the LAA was adsorbed on the surface of the GGBFS particles, which in turn delayed the hydration of the GGBFS, as demonstrated by Fig. 7. Figure 10(b) further demonstrates that the initial amount of LAA adsorbed by the solids increases with the LAA dosage. As more LAA is added, the amount of LAA adsorbed by the GGBFS increases, thus resulting in a stronger retarding effect, as observed in Fig. 2 and 7.

After the initial rapid adsorption, the TOC in all samples continued to decrease at a slow rate for a few more hours. This can be attributed to the GGBFS dissolution and the generation of initial hydration products, which provide more surface area for LAA adsorption. After reaching a minimum, the TOC started to increase slowly due to the high dissolution rate of the GGBFS, which could release some adsorbed LAA back into the aqueous phase. After this period, the TOC decreased slowly until the end of the observation period, indicating the production of more hydration products during this stage.

Effect of LAA on pore solutions of hydrating AAS pastes

Figure 11 presents the concentrations of Ca, Si, and Al. In the absence of LAA (Fig. 11(a)), the Ca concentration increases almost linearly with time within the first 40 minutes. The concentration of Ca reaches its peak at

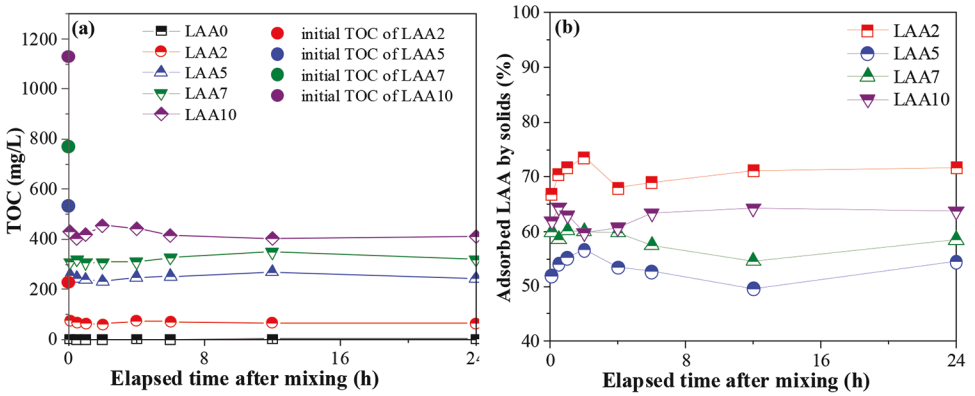

Fig. 10—TOC of aqueous phase of hydrating AAS pastes: (a) TOC; and (b) adsorbed LAA by solids. (Note: 1 mg/L = 8.3 × 10^{-6} lb/gal.)

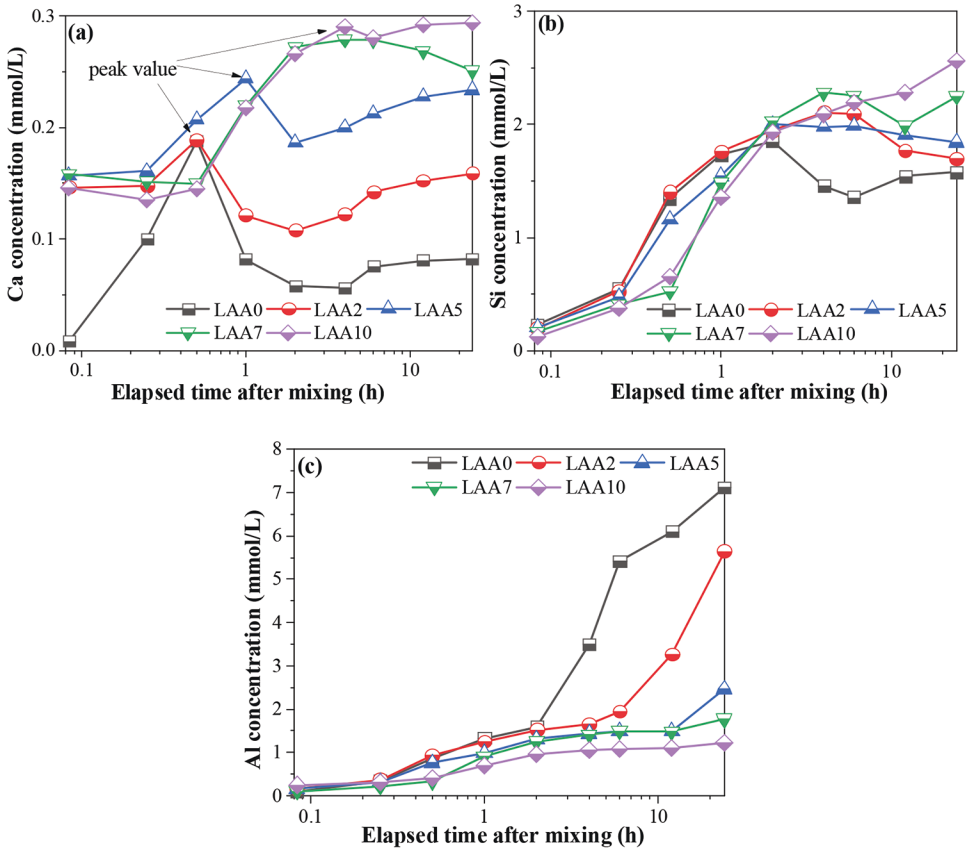

Fig. 11—Concentrations of pore solutions of hydrating AAS pastes: (a) Ca; (b) Si; and (c) Al. (Note: 1 mmol/L = 3.79 mmol/gal.)

40 minutes and subsequently drops rapidly with time to a relatively stable value. This indicates that the supersaturation of Ca^{2+} at the peak is high enough to induce the fast precipitation of the hydration products, consuming the Ca^{2+} in the solution. This fast precipitation of Ca^{2+} ceases once the content of Ca^{2+} drops below the saturation point.

However, the pattern of Ca^{2+} varying with time in the aqueous phase of the fresh AAS is significantly altered by the addition of LAA, as shown in Fig. 11(a). The Ca^{2+} concentrations are already high in all samples with LAA at the beginning of the measurement, indicating a rapid reaction between LAA and Ca^{2+} in the GGBFS, leading to high Ca^{2+} concentrations in these samples immediately after mixing. This can be understood because LAA can chelate Ca^{2+} with its abundant hydroxyl groups,[33] and the dissolved Ca^{2+} from the slag can be tentatively stabilized by the formed LAA-Ca complex without causing rapid precipitation of calcium in all samples. It is interesting to note that the Ca^{2+} concentrations in all samples with LAA are almost the same, suggesting that the initial rapid reaction is controlled by the availability of Ca^{2+}. After the initial reaction, the Ca^{2+} concentrations in all samples remain stable for approximately 20 minutes, indicating that the adsorption of LAA inhibits the dissolution of GGBFS. After this short dormant period, the Ca^{2+} concentrations increase with time in all samples, indicating that the dissolution of GGBFS is underway. Similar to the case of LAA0, the Ca^{2+} concentrations in these samples reach their peaks and start declining with time. However, the peak Ca^{2+} concentration and the corresponding time increase with the dosage of the LAA. When using 0.2% LAA, the value and the arrival time of the peak of the Ca^{2+} concentration are almost identical to those of the LAA0 sample. With more LAA added, the peak value of the Ca^{2+} concentration is higher, suggesting that higher supersaturation is needed to trigger the precipitation of the hydration products. This indicates that LAA can hinder the nucleation of the hydration products, leading to the fact that the nucleation and growth of the hydration products require higher supersaturation of the Ca^{2+} concentrations. This can be further confirmed by the Ca^{2+} concentration in the solution after the fast precipitation of the hydration products, which also increases with the content of LAA.

Figure 11(b) illustrates the Si^{4+} concentration for each mixture. Due to the limitations of ICP-OES in determining Si^{4+} content, the concentration presented is semi-quantitative. It is evident that the addition of LAA does not immediately increase the Si^{4+} concentration in all LAA-containing samples, suggesting the absence of a complex between Si^{4+} and LAA. In addition, the Si^{4+} concentration is found to increase with the LAA dosage, similar to the Ca^{2+} concentration. This is because Si^{4+} is part of the Ca-rich hydration products, such as C-A-S-H and hydrotalcite, and its concentration is closely related to that of Ca^{2+}. Figure 11(c) shows the concentrations of Al^{3+}, which are related to the formation of C-A-S-H and hydrotalcite in AAS. Unlike Ca^{2+} and Si^{4+}, the addition of LAA considerably reduces the concentration of Al^{3+} in the aqueous phases. This suggests that more Al^{3+}

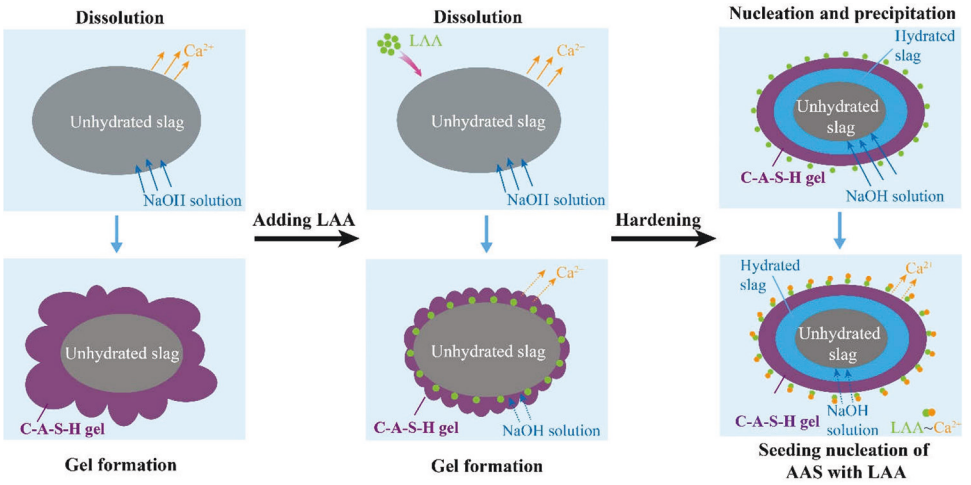

Fig. 12—Mechanism illustration of LAA on hydration of AAS.

is integrated into the structure of hydration products when more LAA is present in the solution.

Mechanism of LAA in enhancing performance of AAS

The preceding results demonstrate that LAA retards the early-age hydration of AAS through a surface-adsorption mechanism on GGBFS grains, primarily as illustrated in Fig. 10. Additionally, due to its chelating ability with ions, the presence of LAA in the pore solutions of AAS maintains the concentration of Ca^{2+} at a supersaturated level. This can further enhance the retarding effect by impeding the precipitation of hydration products at very early stages. Consequently, fewer flocculent products are produced during the initial hydration stage, contributing to enhanced fluidity in the produced AAS mortars, as depicted in Fig. 3.

Basically, the activation of GGBFS begins with the breakdown of its Si-O-Si, Al-O-Si, Ca-O, and Al-O-Al bonds.[34] The presence of NaOH, with its high alkalinity, facilitates the release of Ca^{2+} ions and tetrahedrons of Al-O and Si-O into the pore solutions of AAS. This acceleration results in faster condensation and a shorter operating time.[35,36] However, this rapid setting process can lead to the formation of a high concentration of hydration products around the GGBFS grains, impeding ion diffusion through these products. Consequently, this can have a negative impact on the hydration degree of GGBFS, as early-age hydration of AAS is a diffusion-controlled process.[27] Therefore, when LAA is added as a hydration retarder for AAS, the generation process of hydration products of AAS can be manipulated to be more homogeneous, improving ion diffusion from GGBFS.

Consequently, with the retarding effect and the formation of the LAA-Ca complex, the hydration of GGBFS can be improved for a longer age with the generation of more hydration products, as verified by Fig. 9. Moreover, as have been proclaimed by studies,[15,25,37] the LAA-Ca complex can work as seeds for the hydration of AAS, as illustrated by Fig. 12. This can be the reason for the generation of more products of AAS with LAA, as demonstrated by the mass loss during TG analysis (Fig. 9). As a result, the pore structure of AAS was densified with fewer capillary pores but more gel pores, contributing to less autogenous shrinkage.

CONCLUSIONS

This study explores L-ascorbic acid (LAA) as an environmentally friendly, multifunctional additive for enhancing the performance of NaOH-activated slag materials. Experimental results confirmed that the addition of LAA resulted in prolonged setting time, improved fluidity, increased compressive strength, and reduced autogenous shrinkage of alkali-activated slag (AAS). The adsorption of LAA on ground-granulated blast-furnace slag (GGBFS) grains and the chelating of LAA with Ca^{2+} in the pore solutions of AAS retarded the hydration of AAS. Nevertheless, for a longer curing age, the hydration of GGBFS can be improved for a longer age with the generation of more hydration products owing to the hydration retarding effect. Moreover, the LAA-Ca complex can work as seeds for the hydration of AAS, further enhancing its hydration. As a result, the pore structure of AAS displayed diminished capillary pores with sizes smaller than 100 nm (3.9×10^{-6} in.) but more gel pores, leading to an increase in compressive strength and a decrease in autogenous shrinkage. For instance, the compressive strengths of AAS mortars were improved by 28.9% (3 days) and 19.6% (28 days) with the addition of 0.5% LAA, and the autogenous shrinkage of AAS mortars at 28 days was reduced by 33.3 to 63.7% with the addition of LAA.

In addition, it should be noted that the autogenous shrinkage of AAS is closely related to internal relative humidity, pore structure, pore solution, and elastic modulus.[38,39] A more comprehensive study on the mechanism of autogenous shrinkage reduction owing to LAA is needed in future studies.

AUTHOR BIOS

Peiyuan Chen *is an Associate Professor in the School of Civil Engineering and Architecture at Anhui University of Science and Technology, Huainan, Anhui, China. He received his doctorate in engineering from the University of Science and Technology of China, Hefei, Anhui, China, in 2017. His research interests include civil engineering and green building materials.*

Chunning Pei *is a Graduate Student in the School of Civil Engineering and Architecture at Anhui University of Science and Technology, where he*

received his bachelor's degree in engineering in 2021. His research interests include green building materials and resource use of solid waste materials.

Liheng Zhang *is a PhD Student in the School of Materials Science and Engineering at Tongji University, Shanghai, China. He received his Master of Engineering from Anhui University of Science and Technology in 2022. His research interests include green building materials, resource use of solid waste materials, and concrete admixtures.*

Shangkun Li *is a Graduate Student in the School of Civil Engineering and Architecture at Anhui University of Science and Technology, where he received his bachelor's degree in engineering in 2021. His research interests include green building materials, resource use of solid waste materials, and ultra-high-performance concrete (UHPC) thermal curing.*

Jialai Wang *is a Professor in the Department of Civil, Construction and Environmental Engineering at The University of Alabama, Tuscaloosa, AL. His research interests include concrete modification and functional materials for buildings.*

ACKNOWLEDGMENTS

This study was funded by the U.S. National Science Foundation (1761672 and 2236331) and the National Natural Science Foundation of China (52008003).

REFERENCES

1. Pal, A., "Developing Low-Clinker Ternary Blends for Indian Cement Industry," *Journal of The Institution of Engineers (India): Series A*, V. 99, Sept. 2018, pp. 433-447. doi: 10.1007/s40030-018-0309-4

2. Josa, A.; Aguado, A.; Heino, A.; Byars, E.; and Cardim, A., "Comparative Analysis of Available Life Cycle Inventories of Cement in the EU," *Cement and Concrete Research*, V. 34, No. 8, Aug. 2004, pp. 1313-1320.

3. Chen, P.; Wang, J.; Wang, L.; and Xu, Y., "Perforated Cenospheres: A Reactive Internal Curing Agent for Alkali Activated Slag Mortars," *Cement and Concrete Composites*, V. 104, Nov. 2019, Article No. 103351. doi: 10.1016/j.cemconcomp.2019.103351

4. Juenger, M. C. G.; Winnefeld, F.; Provis, J. L.; and Ideker, J. H., "Advances in Alternative Cementitious Binders," *Cement and Concrete Research*, V. 41, No. 12, Dec. 2011, pp. 1232-1243. doi: 10.1016/j.cemconres.2010.11.012

5. Keulen, A.; Yu, Q. L.; Zhang, S.; and Grünewald, S., "Effect of Admixture on the Pore Structure Refinement and Enhanced Performance of Alkali-Activated Fly Ash-Slag Concrete," *Construction and Building Materials*, V. 162, Feb. 2018, pp. 27-36. doi: 10.1016/j.conbuildmat.2017.11.136

6. Tong, S.; Yuqi, Z.; and Qiang, W., "Recent Advances in Chemical Admixtures for Improving the Workability of Alkali-Activated Slag-Based Material Systems," *Construction and Building Materials*, V. 272, Feb. 2021, Article No. 121647.

7. Alrefaei, Y.; Wang, Y.-S.; and Dai, J.-G., "Effect of Mixing Method on the Performance of Alkali-Activated Fly Ash/Slag Pastes along with Polycarboxylate Admixture," *Cement and Concrete Composites*, V. 117, Mar. 2021, Article No. 103917. doi: 10.1016/j.cemconcomp.2020.103917

8. Luukkonen, T.; Abdollahnejad, Z.; Ohenoja, K.; Kinnunen, P.; and Illikainen, M., "Suitability of Commercial Superplasticizers for One-Part Alkali-Activated Blast-Furnace Slag Mortar," *Journal of Sustainable Cement-Based Materials*, V. 8, No. 4, 2019, pp. 244-257. doi: 10.1080/21650373.2019.1625827

9. Zhang, Y.; Luo, X.; Kong, X.; Wang, F.; and Gao, L., "Rheological Properties and Microstructure of Fresh Cement Pastes with Varied Dispersion Media and Superplasticizers," *Powder Technology*, V. 330, May 2018, pp. 219-227. doi: 10.1016/j.powtec.2018.02.014

10. Łaźniewska-Piekarczyk, B., "The Methodology for Assessing the Impact of New Generation Superplasticizers on Air Content in Self-Compacting Concrete," *Construction and Building Materials*, V. 53, Feb. 2014, pp. 488-502. doi: 10.1016/j.conbuildmat.2013.11.092

11. Alrefaei, Y.; Wang, Y.-S.; and Dai, J.-G., "The Effectiveness of Different Superplasticizers in Ambient Cured One-Part Alkali Activated Pastes," *Cement and Concrete Composites*, V. 97, Mar. 2019, pp. 166-174. doi: 10.1016/j.cemconcomp.2018.12.027

12. Kashani, A.; Provis, J. L.; Xu, J.; Kilcullen, A. R.; Qiao, G. G.; and van Deventer, J. S. J., "Effect of Molecular Architecture of Polycarboxylate Ethers on Plasticizing Performance in Alkali-Activated Slag Paste," *Journal of Materials Science*, V. 49, No. 7, Apr. 2014, pp. 2761-2772. doi: 10.1007/s10853-013-7979-0

13. Palacios, M.; Banfill, P. F. G.; and Puertas, F., "Rheology and Setting of Alkali-Activated Slag Pastes and Mortars: Effect of Organic Admixture," *ACI Materials Journal*, V. 105, No. 2, Mar.-Apr. 2008, pp. 140-148. doi: 10.14359/19754

14. Conte, T., and Plank, J., "Impact of Molecular Structure and Composition of Polycarboxylate Comb Polymers on the Flow Properties of Alkali-Activated Slag," *Cement and Concrete Research*, V. 116, Feb. 2019, pp. 95-101. doi: 10.1016/j.cemconres.2018.11.014

15. Chen, P.; Zhang, L.; Wang, J.; Lou, X.; Huang, L.; and Xu, Y., "Exploring Vitamin-C as a Retarder for Calcium Sulfoaluminate Cement," *Construction and Building Materials*, V. 312, Dec. 2021, Article No. 125334. doi: 10.1016/j.conbuildmat.2021.125334

16. Fuchs-Godec, R.; Pavlovic, M. G.; and Tomic, M. V., "The Inhibitive Effect of Vitamin-C on the Corrosive Performance of Steel in HCl Solutions," *International Journal of Electrochemical Science*, V. 8, No. 1, Jan. 2013, pp. 1511-1519. doi: 10.1016/S1452-3981(23)14115-0

17. Fuchs-Godec, R.; Pavlovic, M. G.; and Tomic, M. V., "The Inhibitive Effect of Vitamin-C on the Corrosive Performance of Steel in HCl Solutions - Part II," *International Journal of Electrochemical Science*, V. 10, No. 12, Dec. 2015, pp. 10502-10512. doi: 10.1016/S1452-3981(23)11275-2

18. Erel-Unal, I., and Sukhishvili, S. A., "Hydrogen-Bonded Multilayers of a Neutral Polymer and a Polyphenol," *Macromolecules*, V. 41, No. 11, June 2008, pp. 3962-3970. doi: 10.1021/ma800186q

19. Andjelković, M.; Van Camp, J.; De Meulenaer, B.; Depaemelaere, G.; Socaciu, C.; Verloo, M.; and Verhe, R., "Iron-Chelation Properties of Phenolic Acids Bearing Catechol and Galloyl Groups," *Food Chemistry*, V. 98, No. 1, 2006, pp. 23-31. doi: 10.1016/j.foodchem.2005.05.044

20. ASTM C191-99, "Standard Test Method for Time of Setting of Hydraulic Cement by Vicat Needle," ASTM International, West Conshohocken, PA, 1999, 6 pp.

21. ASTM C1437-20, "Standard Test Method for Flow of Hydraulic Cement Mortar," ASTM International, West Conshohocken, PA, 2020, 2 pp.

22. ASTM C1698-09(2014), "Standard Test Method for Autogenous Strain of Cement Paste and Mortar," ASTM International, West Conshohocken, PA, 2014, 8 pp.

23. Wang, X.; Wang, W.; Huang, J.; Wang, Z.; Ma, S.; and Liu, Y., "Relationship between Internal Humidity and Drying Shrinkage of Recycled Aggregate Thermal Insulation Concrete Considering Recycled Aggregate Content," *Construction and Building Materials*, V. 355, Nov. 2022, Article No. 129224. doi: 10.1016/j.conbuildmat.2022.129224

24. Brue, F. N. G.; Davy, C. A.; Burlion, N.; Skoczylas, F.; and Bourbon, X., "Five Year Drying of High Performance Concretes: Effect of Temperature and Cement-Type on Shrinkage," *Cement and Concrete Research*, V. 99, Sept. 2017, pp. 70-85. doi: 10.1016/j.cemconres.2017.04.017

25. Fang, Y.; Wang, J.; Qian, X.; Wang, L.; Dong, Y.; and Qiao, P., "Low-Cost, Ubiquitous Biomolecule as a Strength Enhancer for Cement Mortars," *Construction and Building Materials*, V. 311, Dec. 2021, Article No. 125305. doi: 10.1016/j.conbuildmat.2021.125305

26. Provis, J. L.; Brice, D. G.; Buchwald, A.; Duxson, P.; Kavalerova, E.; Krivenko, P. V.; Shi, C.; van Deventer, J. S. J.; and Wiercx, J. A. L. M., "Demonstration Projects and Applications in Building and Civil Infrastructure," *Alkali Activated Materials: State-of-the-Art Report, RILEM TC 224-AAM*, J. L. Provis and J. S. J. van Deventer, eds., Springer, Dordrecht, the Netherlands, 2014, pp. 309-338. doi: 10.1007/978-94-007-7672-2_11

27. Fernández-Jiménez, A., and Puertas, F., "Alkali-Activated Slag Cements: Kinetic Studies," *Cement and Concrete Research*, V. 27, No. 3, Mar. 1997, pp. 359-368. doi: 10.1016/S0008-8846(97)00040-9

28. Zhang, L.; Chen, P.; Xu, Y.; Hu, X.; and Wang, Y., "Upcycling Waste Flavedo into a Bio-Admixture of Set Retarder and Compressive Strength Enhancer for Cement-Based Materials," *Journal of Cleaner Production*, V. 332, Jan. 2022, Article No. 130060. doi: 10.1016/j.jclepro.2021.130060

29. De Filippis, U.; Prud'homme, E.; and Meille, S., "Relation between Activator Ratio, Hydration Products and Mechanical Properties of Alkali-Activated Slag," *Construction and Building Materials*, V. 266, Part A, Jan. 2021, Article No. 120940. doi: 10.1016/j.conbuildmat.2020.120940

30. Ipavec, A.; Gabrovšek, R.; Vuk, T.; Kaučič, V.; Maček, J.; and Meden, A., "Carboaluminate Phases Formation During the Hydration of Calcite-Containing Portland Cement," *Journal of the American Ceramic Society*, V. 94, No. 4, Apr. 2011, pp. 1238-1242. doi: 10.1111/j.1551-2916.2010.04201.x

31. Bernal, S. A.; Rodríguez, E. D.; Mejía de Gutiérrez, R.; Gordillo, M.; and Provis, J. L., "Mechanical and Thermal Characterisation of Geopolymers Based on Silicate-Activated Metakaolin/Slag Blends," *Journal of Materials Science*, V. 46, No. 16, Aug. 2011, pp. 5477-5486. doi: 10.1007/s10853-011-5490-z

32. Melo Neto, A. A.; Cincotto, M. A.; and Repette, W., "Drying and Autogenous Shrinkage of Pastes and Mortars with Activated Slag Cement," *Cement and Concrete Research*, V. 38, No. 4, Apr. 2008, pp. 565-574. doi: 10.1016/j.cemconres.2007.11.002

33. Juenger, M. C. G., and Jennings, H. M., "New Insights into the Effects of Sugar on the Hydration and Microstructure of Cement Pastes," *Cement and Concrete Research*, V. 32, No. 3, Mar. 2002, pp. 393-399. doi: 10.1016/S0008-8846(01)00689-5

34. Krizan, D., and Zivanovic, B., "Effects of Dosage and Modulus of Water Glass on Early Hydration of Alkali–Slag Cements," *Cement and Concrete Research*, V. 32, No. 8, Aug. 2002, pp. 1181-1188. doi: 10.1016/S0008-8846(01)00717-7

35. Bernal, S. A.; Provis, J. L.; Rose, V.; and Mejía de Gutierrez, R., "Evolution of Binder Structure in Sodium Silicate-Activated Slag-Metakaolin Blends," *Cement and Concrete Composites*, V. 33, No. 1, Jan. 2011, pp. 46-54. doi: 10.1016/j.cemconcomp.2010.09.004

36. Shi, C., and Day, R. L., "A Calorimetric Study of Early Hydration of Alkali-Slag Cements," *Cement and Concrete Research*, V. 25, No. 6, Aug. 1995, pp. 1333-1346. doi: 10.1016/0008-8846(95)00126-W

37. Fang, Y.; Wang, J.; Qian, X.; Wang, L.; Chen, P.; and Qiao, P., "A Renewable Admixture to Enhance the Performance of Cement Mortars through a Pre-hydration Method," *Journal of Cleaner Production*, V. 332, Jan. 2022, Article No. 130095. doi: 10.1016/j.jclepro.2021.130095

38. Li, Z.; Chen, Y.; Provis, J. L.; Cizer, Ö.; and Ye, G., "Autogenous Shrinkage of Alkali-Activated Slag: A Critical Review," *Cement and Concrete Research*, V. 172, Oct. 2023, Article No. 107244. doi: 10.1016/j.cemconres.2023.107244

39. Liang, G., and Yao, W., "Effect of Diatomite on the Reaction Kinetics, Early-Age Chemical Shrinkage and Microstructure of Alkali-Activated Slag Cements," *Construction and Building Materials*, V. 376, May 2023, Article No. 131026. doi: 10.1016/j.conbuildmat.2023.131026